ARTICLE

Received 00th January 20xx,

Accepted 00th January 20xx

DOI: 10.1039/x0xx00000x

Pillared lanthanide metal organic frameworks with sinusoidal channels formed from bent mixed-donor phenanthroline based ligands of different length.

Shengyu Wang, [a] Lauren K. Macreadie [b] and Lyall R. Hanton *[a]

Five new lanthanide MOFs were prepared by solvothermal synthesis to investigate the effect of ligand and pillar length using the unsymmetrical mixed-donor ligands **L1H** (4'-(1H-imidazo[4,5-f][1,10]phenanthrolin-2-yl)-[1,1'-biphenyl]-3-carboxylic acid) and **L2H** (3-(1H-imidazo[4,5-f][1,10]phenanthrolin-2-yl)benzoic acid) and linear pillaring ligands H_2BDC (terephthalic acid) and H_2BPDC (3,4-dihydro-[1,1'-biphenyl]-4,4'-dicarboxylic acid). **Nd-MOF1** and **Gd-MOF1**, [M(BDC)(**L2**)]2.5DMA (M = Nd or Gd), were isomorphous. They both presented a 3D pillared framework with **bcu** topology with a paddlewheel SBU and sinusoidal channels. **Nd-MOF2**, [Nd(BDC)(**L1**)].4DMA, has a pseudo-paddlewheel SBU and formed a 3D pillared **pcu** framework where 1D double-chains were crosslinked with BDC to provide sinusoidal channels. **Gd-MOF2**, $[Gd_2(BPDC)_2(\mathbf{L1})_2].9DMA.0.25H_2O$, has a pseudo-paddlewheel SBU and the 1D double-chains were cross-linked by BPDC to form a regular **pcu** 3D network which was interpenetrated and has sinusoidal channels. The solvent rich **Nd-MOF3**, $[Nd_2(BPDC)(\mathbf{L1})_2(DMA)_4](OH)_2.10DMA$, has a pseudo-paddlewheel SBU and formed 1D double-chains which were partially cross linked by BPDC to form a 2D sheet. The bound DMA solvent prevented the extension of these sheets into a 3D framework. Interestingly, the double chains do not interfere with the adoption of a regular topology by the networks. The sinusoidal channels appeared to be a consequence of the unsymmetrical nature of the **L1H** and **L2H** ligands.

Introduction

Metal organic framework (MOF) chemistry has developed into a very productive area of research offering access to unique structural properties such as high surface area, porosity, tuneable and adjustable internal surface properties, and variability of organic and inorganic components of the structures.[1-9] In MOF chemistry, lanthanide MOFs (Ln-MOFs) have become increasingly popular due to their particular set of properties.[10-12] The lanthanide ions compared to transition metal ions often have higher coordination numbers, and bonds which have more ionic character making them less directional and leading to more varied coordination geometries[13, 14] and structures with diverse topologies.[13, 15] An important aspect of using lanthanide ions with the possibility of having an expanded coordination sphere is that default topologies such as diamondoid networks can be avoided.[13, 16, 17] However, the high coordination environment and connectivity of lanthanides can often lead to the formation condensed frameworks which lack solvent accessible space.[14] With careful design of the ligands this can be prevented. In this study the use mixed-donor imidazo[4,5-f]-1,10-phenanthroline based ligands, **L1H** and **L2H**, of different lengths will be explored. These ligands have large π-conjugation which can increase the rigidity of the framework through "double-chain" π-stacking interactions.[18-21] In addition, the imidazole ring present in this type of ligand may provide hydrogen donor or acceptor sites. The ligands **L1H** and **L2H** (Scheme 1) were designed to have 3-substituted carboxylate donor groups instead of the more usual linear 4-substituted carboxylate groups such as HNCP.[18] This 120° kink was introduced into these ligands in an attempt to facilitate the formation of alternative structures. The unsymmetrical natures of the ligands should give more versatility within the structures

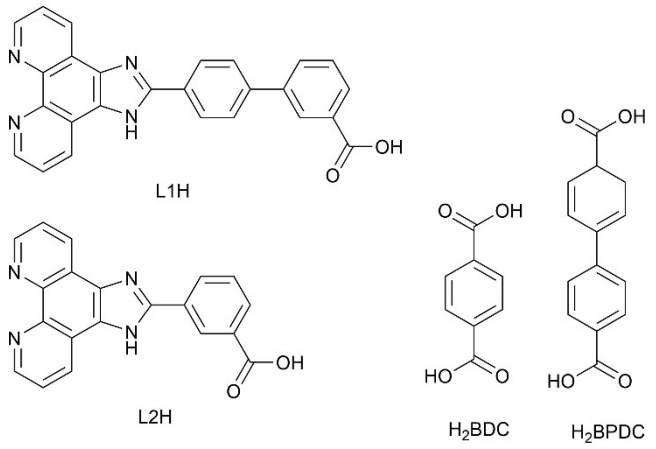

Scheme 1: Mixed-donor ligands and pillaring ligands.

[a] Department of Chemistry, University of Otago, Te Tari Hua-Ruanuku, P. O. Box 56, Dunedin 9054, New Zealand. E-mail: lhanton@chemistry.otago.ac.nz
[b] School of Chemistry, University of New South Wales, Sydney, NSW, Australia.
† Electronic Supplementary Information (ESI) available: Experimental details, characterisation and crystallographic details. CCDC 2352103-2352107. For ESI and crystallographic data in CIF or other electronic format see DOI: 10.1039/x0xx00000x

as it will move away from a simple linear arrangement between ligands and metal ions. However, the unsymmetric nature of these ligands may cause difficulty in the formation of MOFs as the products are less likely to crystalise because they may have lower symmetry and this may hamper crystal formation.[22] In synthesising high coordinate Ln-MOFs using solvothermal processes[23] it is often found that solvent molecules bind directly to the Ln metal ion occupying coordination sites and preventing the extension of the network into higher dimensions.[24] The introduction of simple dicarboxylate pillaring ligands,[25] such as BDC[26-29] and BPDC[30-32] (Scheme 1), into a Ln-MOF structure can replace coordinated solvent molecules leading to a possible extension of the network.[33-35] By using the unsymmetrical linker ligands **L1** and **L2** together with the pillaring ligands BDC and BPDC a systematic study of the effect on Ln-MOF structures of ligand type and length can be undertaken.

In total. there are about 18 structures reported that have used the linear mixed-donor NCP carboxylate ligand with Ln ions.[24, 36-38] Interestingly, most of the structures are coordination polymers, even when pillaring ligands are used. A common feature of all of these structures is the presence of 1D double-chains as a consequence of the large π surface of the NCP ligand. A series of isostructural bi-ligand Ln coordination polymers (Ln = Pr, La, Nd, Sm) based on NCP and pyridine-2,5-dicarboxylate ligands was reported by Zhang.[36] The 1D double-chains are linked by the pyridine-2,5-dicarboxylate ligands into sheets which are H-bonded to form an overall 3D structure. Two interpenetrated Eu-MOFs of the same topology as each other have been reported that were produced from NCP and the pillaring BDC/BPDC carboxylate ligands.[37] The NCP ligands form 1D double-chains with the Eu(III) nodes which are connected by BDC ligands to form a 2D double-layer structure. The adjacent 2D layers are further connected by BDC ligands to form a 3D porous framework. Zhou et al reported two isomorphous 1D Ln coordination polymers (Ln = Sm, Eu) containing NCP double-chains.[38] These 1D double-chains are H-bonded and π-stacked to form a 2D network.

Herein, the crystal structures of five new Ln-MOFs (Ln = Nd, Gd) are reported, namely, **Nd-MOF 1**, **Gd-MOF 1**, **Nd-MOF 2**, **Gd-MOF 2** and **NdMOF3**. All Ln-MOFs, with the exception of **Nd-MOF3**, have the same Ln:ligand:pillar ratio of 1:1:1. **Nd-MOF3**, as a consequence of excess solvent, has a Ln:ligand:pillar of 2:2:1. Unlike the examples discussed above, our strategy has been to use the higher coordination numbers possible with Ln ions, together with the 1:1:1 ratio, to provide structural outcomes which result in 3D MOF formation and solvent accessible volumes. The longer **L1** ligand favoured the formation of double-chain structures that should be more robust and were influenced by the length of the pillar ligand (**Nd-MOF 2**, **Gd-MOF 2** and **Nd-MOF3)**. For example, the longer BPDC pillar gave an interpenetrated structure, **Gd-MOF 2**. Use of the shorter **L2** ligand gave rise to a differently configured SBU and overall MOF topology (**Nd-MOF 1**, **Gd-MOF 1)**. The bridging ligands **L1** and **L2** were designed with a 120° kink arising from the 3-substituted carboxylate donor group. This kink appeared to facilitate the formation of sinusoidal channels in all of the Ln-MOFs leading to solvent accessible volume of between 40-50%. Such sinusoidal channels may point to the future use of these Ln-MOFs as the engineering of sinusoidal channels in MOF structures has been shown to be particularly important in selective CO_2[39] and iodine adsorption[40], separation of gases[41, 42] and separation of organic mixtures.[43, 44]

Experimental

All starting materials were purchased from commercial suppliers and used without any further purification. 1,10-phenanthroline-5,6-dione[45] and 4'-formyl-[1,1'-biphenyl]-3-carboxylic acid[46] were synthesised following a modified literature procedure. All solvents used in the synthetic procedures were of LR grade or better. ^{1}H NMR spectra were collected at 298 K at 400/600 MHz on a Varian 400/JEOL 600-MR NMR spectrometer. Spectra were collected in, DMSO-d_6 and

were referenced to the solvent peak at δ 2.50 ppm. Chemical shifts were reported to the nearest 0.01 ppm and coupling constants (J) to the nearest 0.1 Hz. ^{13}C NMR spectra were collected at 298 K at 151 MHz on a JEOL 600-MR NMR spectrometer. Spectra were collected in DMSO-d_6 and referenced 39.52 ppm. Chemical shifts are reported to the nearest 0.1 ppm. All Electro-spray mass spectrometry (ESMS) was carried out on a Bruker microTOFQ instrument (Bruker Daltronics, Bremen, Germany). Samples were introduced using direct infusion into an ESO source in a negative or positive mode. Each sample averaged for two minutes over a *m/z* range of 50 to 3000 amu. ESMS spectra were processed using Compass software (version 1.3 Bruker Daltronics, Bremen, Germany). X-ray crystallography data were collected on an Agilent SuperNova Diffractometer using mirror monochromated Cu Kα (λ= 1.54184 Å) at 100 K. Crystals were attached to a 0.3 mm CryoLoop with Paratone N oil, supported in a copper mounting pin. The data were processed with CrysAlisPro[47], with a multiscan adsorption correction being applied. The data were solved by direct methods SHELXT[48] and refined on F^2 using all data by full-matric least-spares procedures SHELXL-2014[49]; interfaced through the program WINGX[50]. All nonhydrogen atoms were refined with anisotropic thermal parameters, the hydrogen atoms inserted at calculated positions and rode on the atoms to which they were attached. Detailed analysis of the extended structure was carried out using PLATON[51] and MERCURY[52] (Version **3.5.1**) Crystallographic data are listed in the ESI.

Synthesis of L1H, 1,10-Phenanthroline-5,6-dione (0.301 g, 1.43 mmol) and 4'-formyl-[1,1'-biphenyl]-3-carboxylic acid (0.320 g, 1.41 mmol) were mixed and dissolved in glacial acetic acid (60 mL). The solution was then heated to 80 °C. When solids were fully dissolved, ammonium acetate (2.59 g, 33.6 mmol) was added to the solution. The solution was heated with stirring to 120 °C and refluxed for 4 hours. Then the solution was quenched with ice cold water (100 mL) and cooled. The precipitate was collected via vacuum filtration and washed with water (50 mL), methanol (50 mL), and acetone (50 mL) then dried in an oven at 60 °C. The product was obtained as a yellow-orange powder (0.45 g, 77%). ^{1}H NMR (600 MHz, DMSO-d_6) δ

9.01 (dd, 2H, H-1, 14), 8.93 (dd, 2H, H-3, 12), 8.40 (d, 2H, H-4, 11, J = 12 Hz), 8.30 (s, 1H, H-9), 8.02 (d, 1H, H-8, J = 6 Hz), 7.95 (d, 3H, H-5, 6, 10), 7.81(dd, 2H, H-2, 13), 7.61 (t, 1H, H-7, J = 6 Hz); ^{13}C NMR (151 MHz, DMSO-d_6) δ 172, 168, 150, 148, 146, 144, 140, 132, 130, 127, 123, 121; ES-MS M = $[C_{26}H_{16}N_4O_2]Na^+$, $[M+Na]^+$ found (m/z): 439.11714; calc (m/z) = 439.11655.

Synthesis of L2H, 1,10-Phenanthroline-5,6-dione (0.402 g, 1.90 mmol) and 3-formylbenzoic acid (0.358 g, 2.30 mmol) were mixed and dissolved in glacial acetic acid (60 mL). The solution was then heated to 80 °C. When solids were fully dissolved, ammonium acetate (4.21 g, 54.6 mmol) was added to the solution. The solution was heated with stirring to 120 °C and refluxed for 4 hours. Then the solution was quenched with ice cold water (100 mL) and cooled. The precipitate was collected via vacuum filtration and washed with water (50 mL), methanol (50 mL), and acetone (50 mL) then dried in oven at 60 °C. The product was obtained as a yellow powder (0.62 g, 96%). ^{1}H NMR (600 MHz, DMSO-d_6) δ 13.95 (s, NH), 9.01 (s, 2H, H-1, 10), 8.93 (t, 2H, H-3, 8, J = 12 Hz), 8.88 (s, 1H, H-7), 8.51 (d, 1H, H-4, J = 6 Hz), 8.05 (d, 1H, H-6, J = 6 Hz), 7.84 (dd, 2H, H-2, 9), 7.72 (t, 1H, H-5, J = 6 Hz); ^{13}C NMR (151 MHz, DMSO-d_6) δ 167, 150, 148, 136, 132, 130, 127, 123; ES-MS M = $[C_{20}H_{12}N_4O_2]Na^+$, $[M+Na]^+$ found (m/z): 363.08492; calc (m/z) = 383.08525.

Synthesis of Ln-MOFs, The Ln-MOFs were all synthesised in a similar manner to **Nd-MOF 1**. In all cases only a few good quality crystals could be isolated and in all samples there was an excess of the bridging and pillaring ligands.

Synthesis of Nd-MOF 1, [Nd(BDC)(L2)]2.5DMA. L2H (84.3 mg, 0.247 mmol), $Nd(CF_3SO_3)_3$ (57.3 mg, 0.0968 mmol), and BDC (62.3 mg, 0.372 mmol) were suspended in DMA (2 mL) in a sample vial. The solution was then sonicated at 80 °C until all solids dissolved. The sample vial was placed inside a glass jar and sealed with a cap. The glass jar was then placed inside a metal tube. The metal tube was placed upright in an oven and heated to 100 °C for 48 hours under autogenous pressure, until yellow cubic crystals were formed.

Synthesis of Gd-MOF1, [Gd(BDC)(L2)]2.5DMA. L2H (76.3 mg, 0.224 mmol), $Gd(CF_3SO_3)_3$ (54.7 mg, 0.0905 mmol), and BDC (32.2 mg, 0.193 mmol). Sample heated to 100 °C for 48 hours under autogenous pressure, until yellow cubic crystals were formed.

Synthesis of Nd-MOF2, [Nd(BDC)(L1)].4DMA. L1H (81.9 mg, 0.196 mmol), $Nd(CF_3SO_3)_3$ (39.2 mg, 0.0662 mmol), and BDC (22.4 mg, 0.134 mmol) Sample heated to 100 °C for 72 hours under autogenous pressure, until yellow crystals were formed.

Synthesis of Gd-MOF2, $[Gd_2(BPDC)_2(L1)_2]$.9DMA.0.25H_2O. L1H (45.9 mg, 0.110 mmol), $Gd(CF_3SO_3)_3$ (45.1 mg, 0.0746 mmol), and BPDC (42.9 mg, 0.177 mmol) Sample heated 100 °C for 72 hours under autogenous pressure, until yellow cubic crystals were formed.

Synthesis of Nd-MOF3, $[Nd_2(BPDC)(L1)_2(DMA)_4](OH)_2$.10DMA. L1H (60.3 mg, 0.144 mmol), $Nd(CF_3SO_3)_3$ (58.6 mg, 0.0991 mmol), and BPDC (21.1 mg, 0.0871 mmol) 100 °C for 48 hours under autogenous pressure, until yellow cubic crystals were formed.

Results and discussion

The ligands **L1H** and **L2H** were synthesised in high yield using a two-step process. The precursor 1,10-phenanthroline was first converted into 1,10-phenanthroline-5,6-dione and through the Debus-Radziszewski reaction[53] with the desired aldehyde to produce each ligand. Both **L1H** and **L2H** were characterised by

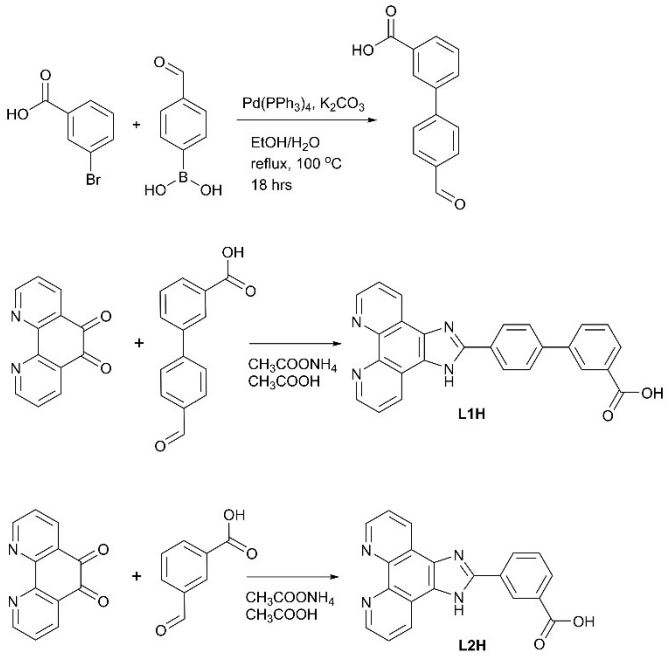

Scheme 2 Top: Synthesis of 4'-formyl-[1,1'-biphenyl]-3-carboxylic acid from adapted literature procedure. Middle : Debus-Radziszewski synthesis of 2-(3-carboxyphenyl-biphenyl)imidazo[4,5-f]1,10-phenanthroline **L1H**. Bottom: Debus-Radziszewski synthesis of 2-(3-carboxyphenyl)imidazo[4,5-f]1,10-phenanthroline **L2H** using the commercially available 3-formylbenzoic acid.

^{1}H NMR, ^{13}C NMR spectroscopy and mass spectrometry.
All attempts at Ln-MOF formation by solvothermal synthesis take place in N,N-dimethylacetamide (DMA) solvent rather than N,N-dimethylformamide (DMF) in order to avoid issues with the formation of formate side products. **L1H** and **L2H** are not soluble on their own in DMA without the addition of a metal salt and use of heating.

Nd-MOF1 and **Gd-MOF1,** X-ray quality crystals of [M(BDC)(**L2**)]nDMA [M = Nd (n=2.5) or Gd (n=3)], **Nd-MOF1** and **Gd-MOF1** were formed from the solvothermal reaction in DMA of **L2H**, H_2BDC and $Nd/Gd(CF_3SO_3)_3$. Both **Nd-MOF1** and **Gd-MOF1** crystallised in the orthorhombic space group *Pbcn*. They both formed 3D MOFs with channels. Since these two structures are isomorphous, only **Gd-MOF1** will be described. The asymmetric unit of the structure contained one Gd(III) ion, one **L2** ligand, and one BDC ligand and one DMA solvent molecule. The Gd(III) ion is eight coordinate, the carboxylate group on one **L2** ligand and the N donor atoms on the phenanthroline of a symmetry related **L2** ligand are chelated in a bidentate fashion to the Gd(III) ion (Fig. 1a). Average Gd-donor bond distances were for Gd-O, 2.367(3) Å, and for Gd-N 2.583(4) Å. There are four BDC ligands chelated in bis-monodentate fashion to the

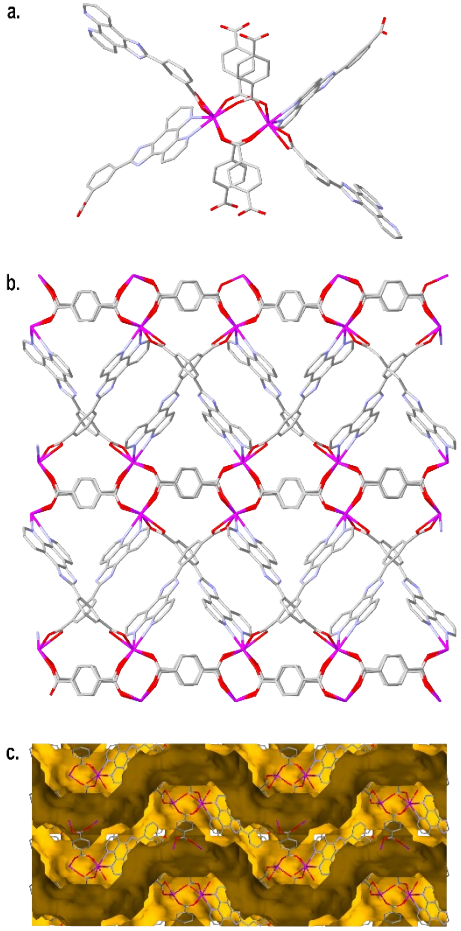

Figure 1: structure of **Gd-MOF1**.(a) coordination environment of Gd ion and the extended SBU with paddlewheel formed by four BDC ligands. (b) view down the *b*-axis showing the 3D framework connected from 2D paddlewheels via **L2** ligands in criss-cross fashion. (c) view of sinusoidal channels running down the *a*-axis. Gd(III) (pink), carbon (grey), oxygen (red), nitrogen (blue).

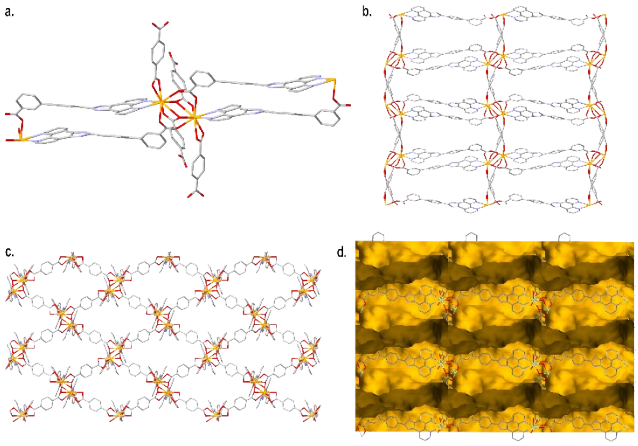

Figure 2: structure of **Nd-MOF2**. (a) view showing the coordination environment of Nd ion, the 1D double-chain formed by four **L1** ligands and pseudo-paddlewheel formed by two **L1** and two BDC ligands. (b) view down the c-axis showing the 1D double-chains connected by BDC ligands in a criss-cross fashion to form the 3D framework. (c) view down the *a*-axis showing BDC ligands linking 1D double-chain into the 3D framework (d) view showing sinusoidal channels running down the *b*-axis. Nd(III) (yellow), carbon (grey), oxygen (red), nitrogen (blue).

Gd(III) ion to complete the coordination environment. These four BDC ligands through their bis-monodentate binding form a pseudo-paddlewheel structure (Fig 1a). The Gd(III) ions of the paddlewheel are generated by a two-fold rotation axis. The two symmetry related Gd(III) ions within the SBU are bridged by the pseudo paddlewheel. The distance between the Gd(III) ions in the SBU paddlewheel is 4.325 Å while for the isomorphous Nd structure the Nd(III) ions in the paddlewheel are 4.364 Å apart. The SBU consists of a paddlewheel arrangement made up with four carboxylate donors from BDC ligands. The N donors from the two **L2** ligands on each symmetry related Gd(III) ions only act as capping ligands for an individual paddlewheel. One of the **L2** ligands chelates through the N donor atoms of the phenanthroline whereas the other symmetry-related **L2** ligand chelates through the 3-substituted carboxylate. The **L2** ligands are perpendicular to each other as a consequence of the 3-substitution of the carboxylate group. The paddlewheel SBUs are connected by the BDC ligands and form a sheet in the *ab* plane. These sheets are connected in a cris-cross manner by **L2** ligands to form a porous 3D structure (Fig 1b). The topological analysis showed an 8-connected 3D framework with the **bcu**[54] topological net and the Schläfli symbol of $4^{24}.6^{4}.$[55] **Gd-MOF1** has sinusoidal channels running along the *c*-axis which if all solvent molecules are removed provided a solvent accessible area of 43.6% of the unit-cell volume (Fig 1c). In addition, the theoretical accessible surface area for N_2 gas (2136.46 m^2 cm^{-3}) and pore volume (3723.34 $Å^3$) were calculated using Zeo++.[56] The SQUEEZE routine of PLATON was used to remove the electron density associated with very disordered solvent molecules which were unable to be modelled in any sensible way. The SQUEEZE routine removed 852 e/cell. This electron density was assigned to 2 DMA molecules per asymmetric unit. Given that the asymmetric unit already contains a complete well-ordered DMA molecule, that means that in total there are 3 DMA molecules in the asymmetric unit. In Nd-MOF 421 the

SQUEEZE routine removed 577 e/cell or 72 e/SBU. This electron density was assigned to 1.5 DMA molecules in the asymmetric unit making 2.5 DMA molecules present overall.

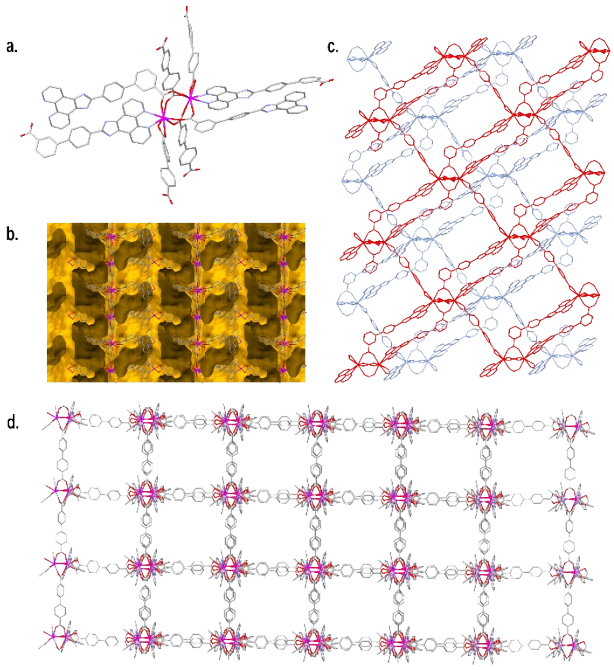

Nd-MOF2, X-ray quality crystals of [Nd(BDC)(**L1**)].4DMA, **Nd-MOF2** were formed from the solvothermal reaction in DMA of **L1H**, H_2BDC and $Nd(CF_3SO_3)_3$. **Nd-MOF2** crystallised in the monoclinic space group $P2_1/c$. It formed a 3D MOF with channels. The asymmetric unit of **Nd-MOF2** consists of one Nd(III) cation, one **L1** ligand, and one BDC ligand. The Nd(III) ion is eight coordinate. The N donor atoms on the phenanthroline of one **L1** ligand and the carboxylate group of one BDC ligand are each chelated to the Nd(III) ion in a bidentate fashion. The carboxylate groups of another two **L1** ligands are chelated in a bis-monodentate manner to each Nd(III) ion which are symmetry related through a centre of inversion. Two more BDC ligands are also chelated in a bis-monodentate manner to each Nd(III) ion to complete the coordination environment (Fig 2a). Interestingly, one oxygen of the carboxylate group of the BDC ligands which bridges the two symmetry related Nd(III) ions gets pulled towards one of the Nd(III) ions giving rise to an asymmetric chelating interaction because of the twist of the paddlewheel bridge. The Nd…O contact distance is 2.83 Å which is longer than any Nd-O bond distance reported in the CSD.[57] The ligand **L1** is severely bowed with the arene carbons ortho to the carboxylate groups at the fourth position being 2.19 Å away from the plane of the phenanthroline ring (Fig. S8). By contrast the BDC ligand is not bowed. The SBU of the structure consists of a pseudo-paddlewheel which is made up with two bis-monodentate symmetry related carboxylate groups from BDC ligands that bridge two symmetry related Nd(III) ions and two bis-monodentate carboxylate groups of two symmetry related **L1** ligands that also bridge two symmetry related Nd(III) ions to complete the paddlewheel (Fig. 2a). The distance between the Nd(III) ions in the SBU paddlewheel is 4.108 Å. The four **L1** ligands contributing to the SBU arrange themselves into a 1D double-chain running along the *a*-axis (Fig. 2b). These 1D chains are connected in a diamond-shaped criss-cross fashion by the four BDC ligands from the SBU (Fig. 2c). In this way a 3D porous MOF structure is generated. The topology of the 6-connected network was determined to be **pcu**[54] with a Schläfli symbol of $4^{20}.6^{6}.^{55}$ **Nd-MOF2** has two different types of channels. There are sinusoidal channels running along the *a*-axis and there are flattened oval shaped channels running along the *c*-axis (Fig. 2d). There are no channels along the *b*-axis. If all solvent molecules are removed this channel system provides a solvent accessible area of 58.3% of the unit-cell volume. The theoretical accessible surface area for N_2 gas (2820.97 m^2 cm^{-3}) and pore volume (3481.49 $Å^3$) were calculated using Zeo++.[56] The SQUEEZE routine of PLATON was used to remove the electron density associated with very disordered DMA solvent molecules which were unable to be modelled in any sensible way. The

Figure 3: structure of **Gd-MOF2**. (a) view of the coordination environment of the Gd ions, the 1D double-chains formed by four **L1** ligands and the pseudo-paddlewheel formed by two **L1** ligands and two BPDC ligands. (b) view of the sinusoidal channels running down the *b*-axis. (c) view down the *b*-axis showing the two fold interpenetration of the framework. (d) view looking down the 1D double-chains running along the diagonal [1 0 1] axis showing BPDC ligands connecting 1D double-chains into the 3D framework. Gd(III) (pink), carbon (grey), oxygen (red), nitrogen (blue).

SQUEEZE routine removed 794 e/cell. This electron density was assigned to 4 DMA molecules per asymmetric unit or Nd ion.

Gd-MOF2, X-ray quality crystals of $[Gd_2(BPDC)_2(\mathbf{L1})_2].9DMA.0.25H_2O$, **Gd-MOF2** were formed from the solvothermal reaction in DMA of **L1H**, H_2BPDC and $Gd(CF_3SO_3)_3$. **Gd-MOF2** crystallised in the monoclinic space group $P2_1/n$. It formed a 3D, doubly interpenetrated MOF with channels. The asymmetric unit consisted of two Gd(III) ions, two **L1** and two BPDC ligands and an unbound DMA and one quarter of a H_2O molecule. The two Gd(III) ions have very similar coordination environments. They are each eight coordinate being bound to three **L1** ligands and three BPDC ligands. One of the **L1** ligands is chelated through the phenanthroline N donors while the remaining two **L1** ligands are bound in a bis-monodentate fashion. In a similar fashion one of the BPDC ligands chelates to a Gd(III) ion while the other two are bound in a bis-monodentate fashion (Fig 3a). Average Gd-donor bond distances were for Gd-O, 2.361(9) Å, and for Gd-N 2.566(9) Å. The two crystallographically distinct **L1** ligands are significantly bowed with the arene carbons ortho to the carboxylate groups at the fourth position being 1.53 (phenanthroline group with N7 and N8) and 1.12 Å (phenanthroline group with N1 and N2) away from the plane of the phenanthroline ring, respectively. For the BPDC ligands, one ligand is not bowed (BPDC with O5 and O6) while for the other ligand, the peripheral carboxylate C tom is 0.70 Å away from the plane phenyl ring of the other carboxylate (Fig. S17). The SBU consists of a pseudo-paddlewheel like structure containing both crystallographically distinct Gd(III) ions. The distance between the Gd(III) ions in the SBU paddlewheel is 4.293 Å. The paddlewheel is formed using the donor moieties of two BPDC and two **L1** ligands. The two BPDC ligands are diametrically opposite each and are arranged in a linear fashion linking adjacent SBUs. The two **L1** ligands are also diametrically opposite each other but because of the 3-substitution of the capping carboxylate group this "kink" causes each **L1** to be approximately parallel to the Gd-Gd vector of the SBU. They point in opposite directions to link adjacent SBUs. The Gd(III) coordination geometry is completed by the N-donor atoms of an **L1** ligand and the O donor atoms of a BPDC ligand. Both ligands bind in a bidentate fashion. While the non-paddlewheel BPDC ligands pillar between each SBU, the **L1** ligands share a role as the capping carboxylate group as the **L1** ligand takes part in the paddlewheel structure of a neighbouring SBU (Fig 3a). This dual role is facilitated by the 3-substition of the carboxylate group in relation to the arrangement of the phenanthroline group. The phenanthroline N donors are not involved in the pseudo-paddlewheel structure. The net result is that again the four **L1** ligands of the SBU are arranged into 1D double-chains running along the diagonal [1 0 1] axis. The 1D chains are connected by four BPDC ligands in an orthogonal

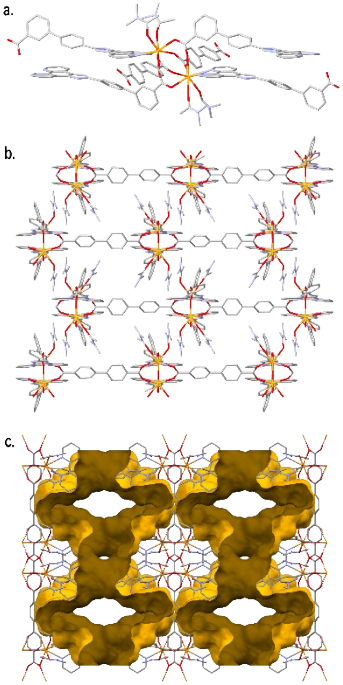

Figure 4: structure of **Nd-MOF3**. (a) view showing the coordination environment of the Nd ions, 1D double-chains formed by four **L1** ligands and the pseudo-paddlewheel formed by two **L1** ligands and two BPDC ligands. (b) view down the 1D double-chains, running along the *a*-axis, connected by BPDC ligands.to form 2D sheets. (c) view of the double-sinusoidal channels running down the *c*-axis. Nd(III) (yellow), carbon (grey), oxygen (red), nitrogen (blue).

criss-cross fashion along the *b* and [-1 0 1] axes. The gives rise to a 3D porous MOF (Fig 3d). The network topology was determined to be **pcu**[54] with a Schläfli symbol of $4^{20}.6^6$ which is the same as for **Nd-MOF2**.[55] The structure was two-fold interpenetrated (Fig 3c). The bulk of the double-chain seemed to prevent any further interpenetration as another network could not be fitted into the available space. However, despite the interpenetration there were 1D channels running along the *b*-axis which if all solvent molecules are removed provided a solvent accessible area of 49.9% of the unit-cell volume (Fig 3b). The theoretical accessible surface area for N_2 gas (2235.03 m^2 cm^{-3}) and pore volume (6387.29 $Å^3$) were calculated using Zeo++.[56] The SQUEEZE routine of PLATON was used to remove the electron density associated with very disordered solvent molecules which were unable to be modelled in any sensible way. The SQUEEZE routine removed 1578 e/cell. This electron density was assigned to 8 DMA molecules per asymmetric unit. Given that the asymmetric unit already contains a complete well-ordered DMA molecule, that means that in total there are 9 DMA molecules in the asymmetric unit.

Nd-MOF3, X-ray quality crystals of $[Nd_2(BPDC)(\mathbf{L1})_2(DMA)_4](OH)_2.10DMA$, **Nd-MOF3** were formed from the solvothermal reaction in DMA of **L1H**, H_2BPDC and $Nd(CF_3SO_3)_3$. **Nd-MOF3** crystallised in the monoclinic space group $P2/c$. It formed 2D sheets which were stacked on top of each other with a slight offset producing a porous MOF with accessible channels. The asymmetric unit of the structure consists of one Nd(III) ion, two bound DMA solvent molecules, one **L1** ligand and half a BPDC ligand. The SQUEEZE routine of PLATON was used to remove the diffuse electron density. The charge balance for the structure was found to be incomplete as a result of the asymmetric unit containing one Nd(III) ion balanced by only the -2 charge from one **L1** and half a BPDC ligand. Thus, the electron density was associated with very

disordered solvent molecules and an anion which was most probably hydroxide formed during the solvothermal reaction. The SQUEEZE routine removed 919 e/cell. This electron density was assigned to one OH^- anion and 5 DMA molecules per asymmetric unit. The Nd(III) ion is eight coordinate. There are two cis-bound solvent DMA molecules occupying two coordination sites. There is one **L1** ligand coordinating through the N donor atoms in a bidentate fashion while two other symmetry related **L1** ligands coordinate through the carboxylate functional group in a bis-monodentate fashion. Finally, there are two BPDC ligands binding in a bis-monodentate manner to complete the coordination geometry about the Nd(III) cation. The SBU of the structure consists of a pseudo-paddlewheel which is made up from the carboxylate groups of two BPDC ligands and two **L1** ligands that are bound to the Nd(III) ions through the carboxylate group (Fig 4a). The distance between the Nd(III) ions in the SBU paddlewheel is 4.481 Å. Both BPDC ligands are diametrically opposite to each other. This paddlewheel arrangement generates a pseudo-square planar array. Finally, the phenanthroline end of the **L1** ligands completes the SBU and as a consequence this generates a 1D double-chain with the symmetry related **L1** ligand associated with the paddlewheel. These 1D double-chain which run along the *a*-axis and are connected by the carboxylate groups of BPDC ligands to form a 2D sheet. The sheets stack on top of each other in a slightly offset manner such that the bound DMA molecules interdigitate between layers (Fig 4b). Despite being a 2D structure, **Nd-MOF3** has small to medium channels running in all three dimensions (Fig 4c). If all solvent molecules and the OH^- anion are removed, the framework has a solvent accessible area of 41.0% of the unit-cell volume. The theoretical accessible surface area for N_2 gas (1884.97 m^2 cm^{-3}) and pore volume (2821.33 $Å^3$) were calculated using Zeo++.[56]

Structural comparison

In this study the comparison of ligand and pillar length on Ln-MOF formation was incomplete. Despite many attempts, using a variety of reaction conditions, to prepare a Ln-MOF using the short **L2** ligand and long BPDC pillar crystalline material was never able to be isolated. This may be because in the **bcu** topology (Fig 1b) the longer BPDC ligand expands distance between SBUs in the 2D sheets making it more difficult for these sheets to be linked by the shorter **L2** ligand. However, there were sufficient permutations of linker and pillar length to make comparison with the MOFs which could be isolated. A key structural feature of the Ln-MOFs containing the longer bridging ligand **L1** is the formation of 1D double-chains as a consequence of **L1** participating in the formation of the paddlewheel SBU. These 1D double-chains are then interconnected by the pillaring ligands, BDC or BPDC, to give the 3D Ln-MOF structure. The exception to this is **Nd-MOF3**. Surprisingly, the double chains do not seem to interfere with the adoption of a regular topology by the networks.

Nd-MOF2 and **Gd-MOF2** consisted of a common bridging ligand, **L1**, but with different pillaring ligands, BDC and BPDC, respectively. The difference in length between the BDC and BPDC ligands resulted in the structure of **Nd-MOF2** being non-interpenetrated while **Gd-MOF2** was interpenetrated. When comparing the two frameworks without considering interpenetration, both frameworks had the same **pcu** topology. Both SBUs of the structures showed a similar pseudo-paddlewheel arrangement that was made up by two **L1** ligands and two pillaring ligands (BDC for **Nd-MOF2** and BPDC ligands for **Gd-MOF2**). Also, an almost identical 1D double-chain arrangement that was made up with four **L1** ligands coming off from the SBU. For **Nd-MOF2**, BDC ligands pillared in a criss-cross diamond shaped fashion whereas in **Gd-MOF2**, BPDC ligands also pillared in a criss-cross fashion but in a more regular way.
Gd-MOF2 and **Nd-MOF3** consisted of the same bridging ligand **L1** and pillaring ligand BPDC. The pseudo-paddlewheel arrangement of the two MOFs was almost identical. However, these two MOFs produced completely different structures in part due to the effect of coordinated DMA solvent. **Gd-MOF2** yielded a 3D interpenetrated framework whereas **Nd-MOF3** produced a 2D sheet structure. **Nd-MOF3** had a charge imbalance in the asymmetric unit with a metal:ligand:pillar ratio of 1:1:0.5. The missing charge, which proved difficult to establish by X-ray crystallography, was assigned to a "free" hydroxide ion. When comparing the SBUs of these two structures, there were four bound BPDC ligands in the SBU of **Gd-MOF2** where two of the BPDC ligands were bidentate and the other two ligands were bis-monodentate. There were only two bound BPDC ligands in the SBU of **Nd-MOF3**, both were bis-monodentate. The rest of the coordination environment on Nd(III) ions was completed by two bound DMA molecules. These bound DMA molecules prevented the formation of a 3D framework by blocking potential coordination sites for chelation by another BPDC ligand allowing the extension of the network.

Nd-MOF1, Gd-MOF1 were isomorphous and both consisted of a bridging ligand **L2** and pillaring ligand BDC. However, the shorter **L2** ligand did not form 1D double-chains in the way that the longer bridging ligand **L1** was able to in the other three structures. The paddlewheel SBU was formed only by four BDC ligands. Most likely the shorter **L2** ligand was not able to be accommodated in the SBU or form double chains without significant steric clashes. Unlike other frameworks, these paddlewheel SBUs were connected in a criss-cross manner by **L2** ligands to form a 3D structure of **bcu** topology.
All structures showed sinusoidal channels in the frameworks with decent void space (between 40 to 50%) when all solvent molecules are removed.

Conclusions

A series of Ln-MOFs (Nd, Gd) was prepared using bridging ligands and pillaring ligands of different length. In the structures there was no observation of 1D double-chains with short **L2** ligand, however, the longer **L1** ligand was found to form double-chains. This gives rise to networks with different topologies. The twisting nature of **L1** ligand was observed across all of the Ln-MOFs. This feature together with the length of the **L1** ligands may be the reason for the formation of the double-chains in

these Ln-MOFs as **L1** can be involved in the paddlewheel formation. When sufficient pillaring ligand is available, solvent molecules are excluded from the coordination sphere of the lanthanide ions leading to the formation of a 3D pillared framework. The presence of both long bridging and pillaring ligand also resulted in the formation of an interpenetrated framework. This phenomenon was not observed in other frameworks with other combinations of bridging and pillaring ligands. The Ln-MOFs all show large potential solvent accessible volumes characterised by sinusoidal channels

Author Contributions

S. Wang: synthesis, formal analysis, data curation, writing – original draft and editing. L. K. Macreadie conceptualization, calculations, review and editing. L. R. Hanton: conceptualization, funding acquisition, supervision, and writing – review and editing. All authors have given approval to the final version of the manuscript.

Conflicts of interest

There are no conflicts to declare.

Acknowledgements

The work was supported by the Department of Chemistry, University of Otago and by the University of Otago publishing bursary to S.W.

References

1. A. Morozan and F. Jaouen, *Energy & Environmental Science*, 2012, **5**, 9269-9290.
2. A. Dhakshinamoorthy, Z. Li and H. Garcia, *Chemical Society Reviews*, 2018, **47**, 8134-8172.
3. P. Kumar, A. Deep and K.-H. Kim, *TrAC Trends in Analytical Chemistry*, 2015, **73**, 39-53.
4. S. Natarajan, S. Manual, P. Mahata, V. K. Rao, P. Ramaswamy, A. Banerjee, A. K. Paul and K. V. Ramya, *Journal of Chemical Sciences*, 2006, **118**, 525-536.
5. M. J. K. Omar M. Yaghi, Christian S. Diercks, in *Introduction to Reticular Chemistry: Metal-Organic Frameworks and Covalent Organic Frameworks*, Wiley-VCH Verlag GmbH & Co. KGaA, 2019, pp. 1-27.
6. K.-Y. Wang, Z. Yang, J. Zhang, S. Banerjee, E. A. Joseph, Y.-C. Hsu, S. Yuan, L. Feng and H.-C. Zhou, *Nature Protocols*, 2023, **18**, 604-625.
7. M. Y. Tsang, A. Sinelshchikova, O. Zaremba, F. Schöfbeck, A. D. Balsa, M. R. Reithofer, S. Wuttke and J. M. Chin, *Advanced Functional Materials*, **n/a**, 2308376.
8. W. Zhang, R. Taheri-Ledari, M. Saeidirad, F. S. Qazi, A. Kashtiaray, F. Ganjali, Y. Tian and A. Maleki, *Journal of Environmental Chemical Engineering*, 2022, **10**, 108836.
9. Z. Chen, K. O. Kirlikovali, L. Shi and O. K. Farha, *Materials Horizons*, 2023, **10**, 3257-3268.
10. X. Li, S. Lu, D. Tu, W. Zheng and X. Chen, *Nanoscale*, 2020, **12**, 15021-15035.
11. Y. Zhang, S. Liu, Z.-S. Zhao, Z. Wang, R. Zhang, L. Liu and Z.-B. Han, *Inorganic Chemistry Frontiers*, 2021, **8**, 590-619.
12. X. Wang, Y. Jiang, A. Tissot and C. Serre, *Coordination Chemistry Reviews*, 2023, **497**, 215454.
13. Y. Chen and S. Ma, *Reviews in Inorganic Chemistry*, 2012, **32**, 81-100.
14. S. Fordham, X. Wang, M. Bosch and H.-C. Zhou, in *Lanthanide Metal-Organic Frameworks*, ed. P. Cheng, Springer Berlin Heidelberg, Berlin, Heidelberg, 2015, pp. 1-27.
15. T. Gorai, W. Schmitt and T. Gunnlaugsson, *Dalton Transactions*, 2021, **50**, 770-784.
16. M. D. Allendorf, V. Stavila, M. Witman, C. K. Brozek and C. H. Hendon, *Journal of the American Chemical Society*, 2021, **143**, 6705-6723.
17. A. H. Assen, K. Adil, K. E. Cordova and Y. Belmabkhout, *Coordination Chemistry Reviews*, 2022, **468**, 214644.
18. H.-Y. Sun, C.-B. Liu, Y. Cong, M.-H. Yu, H.-Y. Bai and G.-B. Che, *Inorganic Chemistry Communications*, 2013, **35**, 130-134.
19. C. J. Setter, M. B. Price, L. Conte, W. Schmitt, S. R. Batten, C. Richardson, M. R. Hill, R. Babarao and L. K. Macreadie, *Chemical Communications*, 2020, **56**, 13377-13380.
20. L. Martins, L. K. Macreadie, D. Sensharma, S. Vaesen, X. Zhang, J. J. Gough, M. O'Doherty, N.-Y. Zhu, M. Rüther, J. E. O'Brien, A. L. Bradley and W. Schmitt, *Chemical Communications*, 2019, **55**, 5013-5016.
21. L.-F. Yang, Z.-P. Zhang, Y.-L. Li, S.-T. Cai, Z.-Y. Li, Y.-R. Shen, Z.-Y. Zhang, J.-Y. Lin, Y.-C. Ou and J.-Z. Wu, *CrystEngComm*, 2024, **26**, 4235-4240.
22. P. J. Steel, *Acc Chem Res*, 2005, **38**, 243-250.
23. Y. Huo, S. Xiu, L.-Y. Meng and B. Quan, *Chemical Engineering Journal*, 2023, **451**, 138572.
24. S. Zhang, Y. Yang, Z.-Q. Xia, X.-Y. Liu, Q. Yang, Q. Wei, G. Xie, S.-P. Chen and S.-L. Gao, *Inorganic Chemistry*, 2014, **53**, 10952-10963.
25. F. ZareKarizi, M. Joharian and A. Morsali, *Journal of Materials Chemistry A*, 2018, **6**, 19288-19329.
26. H. Chun, D. N. Dybtsev, H. Kim and K. Kim, *Chemistry – A European Journal*, 2005, **11**, 3521-3529.
27. D. N. Dybtsev, H. Chun and K. Kim, *Angewandte Chemie International Edition*, 2004, **43**, 5033-5036.
28. V. Safarifard and A. Morsali, *CrystEngComm*, 2014, **16**, 8660-8663.
29. H.-R. Wang and S.-J. Liu, *Synthesis and Reactivity in Inorganic, Metal-Organic, and Nano-Metal Chemistry*, 2016, **46**, 1422-1425.
30. S.-S. Chen, J. Fan, T.-a. Okamura, M.-S. Chen, Z. Su, W.-Y. Sun and N. Ueyama, *Crystal Growth & Design*, 2010, **10**, 812-822.
31. T. Yamada, S. Iwakiri, T. Hara, K. Kanaizuka, M. Kurmoo and H. Kitagawa, *Crystal Growth & Design*, 2011, **11**, 1798-1806.
32. B.-Q. Ma, K. L. Mulfort and J. T. Hupp, *Inorganic Chemistry*, 2005, **44**, 4912-4914.
33. Y. Cui, Y. Yue, G. Qian and B. Chen, *Chemical Reviews*, 2012, **112**, 1126-1162.
34. W. Lu, Z. Wei, Z.-Y. Gu, T.-F. Liu, J. Park, J. Park, J. Tian, M. Zhang, Q. Zhang, T. Gentle Iii, M. Bosch and H.-C. Zhou, *Chemical Society Reviews*, 2014, **43**, 5561-5593.
35. Y.-X. Tan, Y.-P. He and J. Zhang, *Inorganic Chemistry*, 2012, **51**, 9649-9654.

36. X.-J. Zhang, W.-K. Li, W.-T. Zhang, G.-B. Che, X.-Y. Li, Y. Qiao and C.-C. Zhao, *Inorganic Chemistry Communications*, 2015, **51**, 122-125.
37. Y. Qiao, Z.-M. Li, X.-B. Wang, W.-S. Guan, L.-H. Liu, B. Liu, J.-K. Wang, G.-B. Che, C.-B. Liu and X. Lin, *Inorganica Chimica Acta*, 2018, **471**, 397-403.
38. X. Zhou, J.-L. Peng, C.-Y. Wen, Z.-Y. Liu, X.-H. Wang, J.-Z. Wu and Y.-C. Ou, *CrystEngComm*, 2017, **19**, 6533-6539.
39. A. M. Plonka, D. Banerjee, W. R. Woerner, Z. Zhang, J. Li and J. B. Parise, *Chemical Communications*, 2013, **49**, 7055-7057.
40. S. S. Lobanov, J. A. Daly, A. F. Goncharov, X. Chan, S. K. Ghose, H. Zhong, L. Ehm, T. Kim and J. B. Parise, *The Journal of Physical Chemistry A*, 2018, **122**, 6109-6117.
41. S. Gautam and D. Cole, *C*, 2023, **9**, 116.
42. V. J. Witherspoon, J. Xu and J. A. Reimer, *Chemical Reviews*, 2018, **118**, 10033-10048.
43. R. Krishna, *Separation and Purification Technology*, 2019, **215**, 227-241.
44. R. Krishna, *ACS Omega*, 2020, **5**, 16987-17004.
45. R. Satapathy, H. Padhy, Y.-H. Wu and H.-C. Lin, *Chemistry – A European Journal*, 2012, **18**, 16061-16072.
46. R. R. Nagawade and D. B. Shinde, *Journal of Heterocyclic Chemistry*, 2010, **47**, 33-39.
47. C. P. Agilent and P. CrysAlis, *Yarnton, Oxfordshire, England*, 2014, **2014**.
48. G. Sheldrick, *Acta Crystallographica Section A*, 2015, **71**, 3-8.
49. G. Sheldrick, *Acta Crystallographica Section C*, 2015, **71**, 3-8.
50. L. Farrugia, *Journal of Applied Crystallography*, 1999, **32**, 837-838.
51. A. Spek, *Journal of Applied Crystallography*, 2003, **36**, 7-13.
52. C. F. Macrae, P. R. Edgington, P. McCabe, E. Pidcock, G. P. Shields, R. Taylor, M. Towler and J. van de Streek, *Journal of Applied Crystallography*, 2006, **39**, 453-457.
53. J. A. Hernandez Munoz, J. J. Junior and F. Martins da Silva, *Current Organic Synthesis*, 2014, **11**, 824-834.
54. V. A. Blatov, A. P. Shevchenko and D. M. Proserpio, *Crystal Growth & Design*, 2014, **14**, 3576-3586.
55. O. V. Dolomanov, A. J. Blake, N. R. Champness and M. Schröder, *Journal of Applied Crystallography*, 2003, **36**, 1283-1284.
56. T. F. Willems, C. H. Rycroft, M. Kazi, J. C. Meza and M. Haranczyk, *Microporous and Mesoporous Materials*, 2012, **149**, 134-141.
57. C. R. Groom, I. J. Bruno, M. P. Lightfoot and S. C. Ward, *Acta Crystallographica Section B*, 2016, **72**, 171-179.